A rapid microglial metabolic response controls metabolism and improves memory

Anne Drougard[1,2,10], Eric H Ma[3], Vanessa Wegert[1,2], Ryan Sheldon[4], Ilaria Panzeri[1,2], Naman Vatsa[5], Stefanos Apostle[1], Luca Fagnocchi[1], Judith Schaf[2], Klaus Gossens[2], Josephine Völker[2], Shengru Pang[6], Anna Bremser[2], Erez Dror[2], Francesca Giacona[1], Sagar[2,7], Michael X Henderson[5], Marco Prinz[6,8,9], Russell G Jones[3], J. Andrew Pospisilik[1,2,10]

[1] Department of Epigenetics, Van Andel Research Institute, 333 Bostwick Ave, 49503, Grand Rapids, MI, USA

[2] Max Planck Institute of Immunobiology and Epigenetics, Stübeweg 51, 79108 Freiburg, Germany

[3] Department of Metabolism and Nutritional Programming, Van Andel Research Institute, 333 Bostwick Ave, 49503, Grand Rapids, MI, USA

[4] Metabolomics and Bioenergetics Core, Van Andel Research Institute, 333 Bostwick Ave, 49503, Grand Rapids, MI, USA

[5] Department of Neurodegenerative Sciences, Van Andel Research Institute, 333 Bostwick Ave, 49503, Grand Rapids, MI, USA

[6] Institute of Neuropathology, Medical Faculty, University of Freiburg, Freiburg, Germany

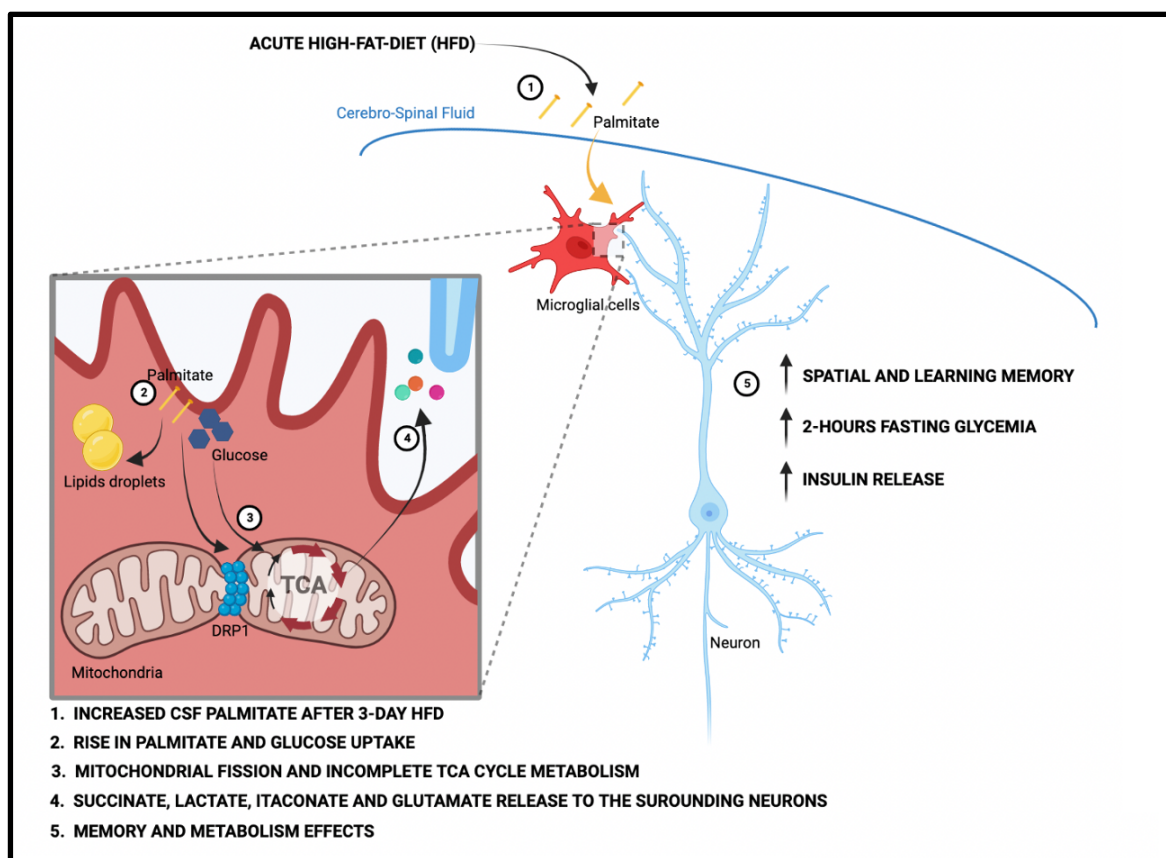[7] Department of Medicine II, University Hospital Freiburg, Freiburg, Germany

[8] Centre for NeuroModulation (NeuroModBasics), University of Freiburg, Freiburg, Germany

[9] Signaling Research Centers BIOSS and CIBSS, University of Freiburg, Freiburg, Germany

[10] Correspondence to: andrew.pospisilk@vai.org, anne.drougard@vai.org

ABSTRACT

Chronic high-fat feeding triggers widespread metabolic dysfunction including obesity, insulin resistance, and diabetes. While these ultimate pathological states are relatively well understood, we have a limited understanding of how high-fat intake first triggers physiological changes. Here, we identify an acute microglial metabolic response that rapidly translates intake of high-fat diet (HFD) to a surprisingly beneficial effect on spatial and learning memory. Acute high-fat intake increases palmitate levels in cerebrospinal fluid and triggers a wave of microglial metabolic activation characterized by mitochondrial membrane activation, fission and metabolic skewing towards aerobic glycolysis. These effects are generalized, detectable in the hypothalamus, hippocampus, and cortex all within 1-3 days of HFD exposure. In vivo microglial ablation and conditional DRP1 deletion experiments show that the microglial metabolic response is necessary for the acute effects of HFD. ^{13}C-tracing experiments reveal that in addition to processing via β-oxidation, microglia shunt a substantial fraction of palmitate towards anaplerosis and re-release of bioenergetic carbons into the extracellular milieu in the form of lactate, glutamate, succinate, and intriguingly, the neuro-protective metabolite itaconate. Together, these data identify microglial cells as a critical nutrient regulatory node in the brain, metabolizing away harmful fatty acids and liberating the same carbons instead as alternate bioenergetic and protective substrates. The data identify a surprisingly beneficial effect of short-term HFD on learning and memory.

1. INCREASED CSF PALMITATE AFTER 3-DAY HFD
2. RISE IN PALMITATE AND GLUCOSE UPTAKE
3. MITOCHONDRIAL FISSION AND INCOMPLETE TCA CYCLE METABOLISM
4. SUCCINATE, LACTATE, ITACONATE AND GLUTAMATE RELEASE TO THE SUROUNDING NEURONS
5. MEMORY AND METABOLISM EFFECTS

INTRODUCTION

The central nervous system (CNS) plays a critical role in regulating glucose and energy homeostasis by sensing, integrating, and responding to peripheral signals [1]. Our understanding of CNS control over energy balance is mostly derived from investigation of distinct functional sets of hypothalamic neurons and their interactions with the periphery[2]. In addition, a growing body of evidence supports an important role for glial cells in regulating energy balance [3]. For example, astrocytes can regulate energy balance by processing glucose into lactate, which is then released to fuel and modulate surrounding neurons [4],[5],[6],[7]. These latter findings demonstrate how metabolic intermediaries from the neuronal niche can directly influence CNS output.

Microglia are the third most abundant glial cell in the brain. Developmentally, they are derived from the yolk sac and are considered CNS immune cells. Like the peripheral immune compartment, microglia activation has been implicated in metabolic disease pathogenesis [8],[9],[10]. Specifically, microglia in the mediobasal hypothalamus (MBH) become activated under conditions of chronic high-fat feeding in a process termed 'microgliosis'. High fat diet (HFD)-induced activation has been associated with moderate increases in cytokine gene expression [8, 11] and pioneering studies testing both genetic manipulation of microglial NF-kB and microglial depletion with PLX5622 suggest that microglial activation is necessary for the metabolic impairments triggered by chronic HFD [9]. Recent evidence suggests a role for microglial mitochondrial alterations (fission) that can be detected within days of high fat diet (HFD) administration [10]. Microglia outside the hypothalamus also activate upon chronic HFD exposure [12, 13] and associate with cognitive impairment [14, 15]. A key outstanding question in the field, then, is how high-fat feeding first triggers microglial activation.

Here, we find that microglia rapidly and directly sense the switch to dietary fat within a single feeding cycle. By three days, HFD increases microglial mitochondrial membrane potential, inhibits complex II activity, and skews mitochondria towards fission. Using cerebrospinal fluid (CSF) metabolomics we demonstrate that microglia are directly exposed to increased palmitate and stearate levels within hours of the feeding switch, and using ^{13}C-tracer studies, we find that microglia robustly metabolize fatty acids via β-oxidation. Interestingly, we find the same acute microglial metabolic response (aMMR) beyond the hypothalamus *in vivo,* in the hippocampus and cortex. aMMR is largely independent of transcriptional changes, and intriguingly, we find that it improves spatial and learning memory. Microglial depletion experiments and microglia-specific DRP deletion show that microglia and more specifically microglial mitochondrial fission, are necessary for the immediate glucose homeostatic responses and memory improvements to HFD. The data thus identify an acute non-transcriptional microglial metabolic pathway that couples detection of acute increases in dietary fat to changes in whole body metabolism and memory.

RESULTS

Acute HFD-induced metabolic changes are microglia dependent

To understand the nature of the immediate high-fat feeding response, we characterized the physiological effects of acute HFD (3d ad libitum feeding) in cohorts of C57BL/6J mice **(Fig 1A)**. Metabolically healthy mice exhibit rapid metabolic shifts on this timescale, including fasting and post-absorptive (2-hr fast) hyperglycemia and an elevated insulin response to glucose (**Fig 1B-E, Suppl Fig S1A-B**) [16, 17]. Glucose excursions, as revealed by baseline-correction, and insulin tolerance test results are minimally impacted upon acute HFD (**Suppl Fig S1C**), an important contrast to chronic HFD [18]. These acute changes in glycemic control are transient, returning to homeostatic levels within one week of a return to normal chow ('Reverse Diet'; **Fig 1C-E**) and are not associated with substantial body weight gain (**Suppl Fig S1D**). To test whether microglia contribute to the induction of these acute HFD-induced effects, we treated mice with the microglia-ablating drug PLX-5622 [19] for 7-9 days and repeated the 3d HFD metabolic assessment. PLX-5622 treatment depleted hypothalamic microglia by >95% across animals (**Fig 1F**) and prevented both the acute HFD-driven insulin hypersecretion and post-absorptive glucose excess (**Fig 1C-E**). Hyperglycemia associated with over-night fasting was unaffected by microglial depletion (**Fig 1C**). The latter indicates that acute HFD triggers microglia-dependent and independent metabolic effects. Thus, microglia are required for metabolic changes induced by the transition to high-fat feeding.

A rapid Microglial Mitochondria Response to high fat diet

Long-term exposure to HFD has previously been associated with hypothalamic microgliosis (increased number and activation of $CD45^{lo};CD11b^+$ microglia) and monocyte infiltration ($CD45^{hi};Cd11b^+$) [9]. Examination of 3d HFD responses in both wild-type animals and animals harboring a microglia-restricted EYFP lineage reporter showed no evidence of either increased hypothalamic microglial proliferation (**Suppl Fig S1E**) or monocyte infiltration (**Suppl Fig S1F**). Similarly, using one of the most sensitive scRNAseq protocols available (CEL-Seq2), we found no evidence of a significant microglial transcriptional response upon 3d HFD. The latter analysis included searches for changes in heterogeneity, skewing across sub-states, and appearance of new cell sub-states (**Fig 1G, Suppl Fig S1G**). The lack of response is especially clear when juxtaposed to experimental autoimmune encephalomyelitis (EAE)-triggered responses performed using the same purification and sequencing protocols in the same laboratory (EAE; **Fig 1G**). Thus, the central effects of acute HFD are distinct from those of chronic HFD, and have little to no effect on microglial expansion, transcription, heterogeneity, or inflammation in the hypothalamus.

A deep body of literature has highlighted how cellular metabolic changes are necessary and sufficient mediators of cell-type specific function, work pioneered recently by the immunometabolism community[20]. We tested whether such changes in cellular metabolism might underpin the microglial response to acute high-fat feeding. Interestingly, mitochondrial membrane potential was increased in

primary MBH microglia sorted from animals administered a 3d HFD (Mitotracker Deep Red; **Fig 2A-B**). Co-staining in the same samples showed no evidence of altered mitochondrial mass (Mitotracker Green; **Fig 2C**). This acute microglial metabolic response (aMMR) was detectable within 12 hours of high-fat feeding (**Fig 2B**). aMMR appeared transient and distinct from the effects induced by chronic HFD. Specifically, parallel measures showed no induction of membrane potential in 4-week HFD animals (**Fig 2B**). Thus, microglia respond to acute dietary fat through a relatively restricted mitochondrial response.

To understand the inputs that might trigger the aMMR response, we performed targeted metabolomics of cerebrospinal fluid (CSF) (**Fig 2D; Suppl Table 1**). Overall, relatively few metabolites change upon 3d HFD. Nicotinamide-N-oxide was the only metabolite that decreased significantly. Six metabolites increased upon 3d HFD including methylmalonate, isovalerylcarnitine, nicotinic acid, glutarylcarnitine, and notably, the fatty acids palmitate (hexadecanoic acid) and stearate (octadecanoic acid). Palmitate and stearate, the only two metabolites that changed by >2-fold, are highly enriched in the HFD itself (Research Diets D12492) suggesting that microglia respond directly to dietary fatty acid levels.

To test whether these observed fatty acid changes in the CSF might directly trigger aMMR, we examined the primary microglial response to palmitate *in vitro* using neonatal microglia (**Fig S2A-B**). Palmitate had no effect on either baseline or maximal oxygen consumption under standard culture conditions (**Fig 2E**). That said, when added in conjunction with succinate (to prime complex II-mediated OxPhos), palmitate-treated microglia were unable to utilize succinate. Acute palmitate therefore appears to rapidly compromise or saturate complex II function and prevent utilization of substrates routed through complex II. Consistent with these *in vitro* findings, fresh primary microglia from 3d HFD animals failed to respond to complex II-specific mitochondrial stimuli (Rotenone + Succinate; **Fig 2F**) validating the findings in adult, *ex vivo* contexts. Consistent with the *in vivo* observations above, *in vitro* palmitate exposure decreased microglial mitochondrial length within 24 hours, indicating that fatty acid exposure itself is sufficient to trigger mitochondrial fission in a cell autonomous manner (**Fig 2G upper panels**). Collectively, these responses were independent of any detectable mitoSOX-activating ROS release (**Fig S2C**), and, were associated with recruitment of the mitochondrial fission regulator DRP1 (**Fig 2H**). A 24h exposure to the mono-unsaturated fatty acid oleate failed to elicit a comparable fission response (**Fig 2G**), and, acute palmitate exposure had no effects on microglial cytokine release *in vitro* (IL6, IL1β, TNFa; **Fig S2E**). Thus, acute fatty acid exposure recapitulates aMMR in vitro including selective loss of complex II activity and lack of significant inflammatory cytokine response.

aMMR is required for diet induced homeostatic rewiring *in vivo*

We next tested whether microglial mitochondrial dynamics are required for the *in vivo* metabolic responses to 3d HFD. We generated tamoxifen-inducible, microglial-*Drp1* knockout mice ($Drp1^{MGKO}$) by crossing $Drp1^{fl/fl}$ animals with a Cx3cr1^{creER} transgenic line [21, 22]. $Drp1^{MGKO}$ animals were born at Mendelian ratios and grow normally. Tamoxifen injection followed by 4 weeks washout generated the intended Drp1-deletion (**Fig 3 A- B, Suppl Fig 3A**) [22].

Body weight, fat mass and lean mass regulation were normal both before and after tamoxifen injection in $Drp1^{MGKO}$ mice, indicating that microglial DRP1 (and by extension microglial mitochondrial fusion) is dispensable for body weight regulation under standard conditions (**Suppl Fig 3B-C**). These data are consistent with literature suggesting that microglia do not substantially participate in body mass regulation [23]. $Drp1^{MGKO}$ mice also showed normal glucose and insulin tolerance (**Fig 3D**) indicating that microglial mitochondrial dynamics are also dispensable for baseline control of glucose homeostasis. Importantly, whereas 3d HFD triggered post-absorptive hyperglycemia and enhanced glucose-induced insulin release in control animals, $Drp1^{MGKO}$ failed to mount a comparable whole body metabolic response (**Fig 3E**). Consistent with the data from **Fig 1**, the 3d HFD-induced-hyperglycemia that is observed under overtly catabolic conditions, which we found to be microglia *independent* (**Fig 1C**), was still present in $Drp1^{MGKO}$ animals (**Fig 3E**). These data reinforce the conclusion that the metabolic responses to acute HFD are highly specific and include both microglia-dependent and independent mechanisms. Thus, microglial mitochondrial dynamics are required for the immediate *in vivo* homeostatic response to 3d HFD.

Microglia take up and metabolize free fatty acids

Based on BODIPY fluorescence, we found that primary microglia increase lipid droplet numbers within 24h of *in vitro* exposure to palmitate (200uM; **Fig 4A**), suggesting a capacity to take up and process fatty acids. To characterize the microglial consequences of fatty acid uptake we used stable isotopic tracer labelling and directly quantified U-[^{13}C]-palmitate (^{13}C-palmitate) processing in both control (BSA treated) and 24h palmitate pre-exposed microglia. Primary microglia incubated with ^{13}C-palmitate for 4 hours, washed and subjected to GCMS or LCMS-based metabolomics (**Fig 4B**). Focusing first on the control microglia we observed significant palmitate uptake and incorporation into downstream metabolites (**Fig 4C- F; and Fig 4O**). This is the first definitive demonstration to our knowledge that microglia metabolize fatty acids. ^{13}C-palmitate label was processed to palmitoylcarnitine and acetylcarnitine indicating that microglial fatty acid metabolism acts via the canonical CPT1/CPT2 pathway, moving carbons from outside the mitochondria into the inner mitochondrial matrix (**Fig 4C, suppl Fig S4A**). ^{13}C-labelling was also found in ^{13}C-acetylserine, indicating that palmitate is processed through β-oxidation and that it contributes to the acetyl-coA pool (**Fig 4D, suppl Fig S4B**). Label was detected in all measured TCA cycle intermediates (**Fig 4E, suppl Fig S4C**). Examination of labelling ratios of TCA intermediates and glutamate indicated that microglia push a substantial fraction of palmitate-derived carbons out of the TCA (alpha-ketoglutarate (a-KG) to glutamate) rather than processing them further through the whole TCA cycle (towards malate) (**Fig 4E-F, suppl Fig S4D**). This is a relatively unique pattern of substrate routing. Thus, microglia store and metabolize palmitate for both energy-producing and anaplerotic reactions.

Palmitate induces a novel microglial lactate/succinate/itaconate release pathway.

We next evaluated the effect of the cold palmitate pretreatment on substrate routing and utilization, our model for understanding aMMR. Palmitate *pretreatment* interestingly increased labelling of palmitoylcarnitine, acetylcarnitine and acetylserine, demonstrating that 24h palmitate exposure accelerates β-oxidation (**Fig 4C-D, suppl Fig S4A-B**). The pre-exposure enhanced m+2 label enrichment at a-KG and glutamate without impacting other TCA intermediates (**Fig 4E-F, suppl Fig S4C-D**) indicating that fatty acid exposure further increases microglial substrate routing to glutamate and anaplerosis. Tracer measurements made in extracellular media conditioned from the same cells revealed that 24h palmitate treatment triggered release of glutamate, succinate, and intriguingly itaconate (**Fig 4G-I**), an immunomodulatory metabolite known to inhibit succinate dehydrogenase (Complex II) [24] and recently shown to be neuroprotective [25]. These findings are consistent with the complex II inhibition observed above upon 3d HFD/palmitate treatment and suggest that itaconate-dependent inhibition of complex II inhibition limits the bioenergetic utilization of fatty acids by microglia, sparing the carbons for release to the cell exterior. Collectively, the data therefore indicate that microglia sense and process fatty acids to generate alternative metabolites for surrounding cells (**Fig 4O**).

We next tested whether the effects of 24h palmitate exposure were specific to palmitate-derived carbons or generalizable to other substrates. We repeated the same experiment, instead replacing U-[^{13}C]-palmitate with U-[^{13}C]-glucose (**Fig 4B**). Under control conditions, microglia exhibited strong glucose uptake, glycolysis and incorporation of glucose-label into TCA intermediates (**Fig 4J, suppl Fig S4E**). Substantial ^{13}C labelling was detected in pyruvate, citrate, a-KG, malate, and again in glutamate, confirming that the unexpected TCA shunt toward glutamate/glutamine pathway is a unique characteristic of the microglial metabolic fingerprint. Importantly, as with palmitate tracing, ^{13}C-glucose-derived metabolites were detected *extracellularly* in the form of glutamate, itaconate and succinate, as well as in extracellular lactate (m+3) (**Fig 4K-N**). Palmitate *pretreatment* increased all of these signatures, including glucose uptake (**Fig 4J**), lactate labelling and lactate release. aMMR is therefore characterized by induction of a Warburg-like metabolic signature (**Fig 4N**). Interestingly, as with palmitate-tracing experiments, fatty acid pretreatment increased release of tracer-labeled itaconate and succinate into the extracellular media (**Fig 4L-M**). Collectively, these data identify microglia as a novel metabolic node able to take-up potentially harmful free fatty acids and repurpose them to fuel surrounding cells in the form of lactate and anaplerotic substrates (**Fig 4O**).

Acute HFD induces widespread MMR and rapid modulation of spatial and learning memory

Changes in neuronal function have previously been linked to lactate provided by glucose metabolism in astrocytes[26]. To determine if the substrates released by microglia have the potential to directly influence neurons, we incubated primary neuron cultures (Suppl **Fig S5A**) with conditioned media from the microglial ^{13}C-glucose tracing experiments (ie. media containing ^{13}C-glucose-derived isotopically labeled lactate, itaconate, succinate, citrate). As a control for direct uptake of residual ^{13}C-glucose, we treated

parallel neuronal cultures with the fresh ^{13}C-glucose tracing media originally added to the microglia. Intriguingly, and consistent with literature documenting poor direct glucose utilization by neurons [27], we found robust m+3 lactate (and other metabolites) in cells treated with microglial conditioned media, at levels that far exceeded labelling triggered by glucose tracer alone (**Fig 5A,** middle column vs left column)(**Suppl Fig S5B**). These data demonstrate that microglia can contribute carbon substrate for neuronal use, and, they highlight the relative importance of this process compared to uptake of pure glucose. The data identify a route through which aMMR likely alters neuronal function.

The majority of literature relating HFD-associated microglial function to metabolic regulation is focused on the hypothalamus, a region of the brain that exhibits an unusually leaky blood brain barrier [8, 28]. Given our findings that CSF free fatty acid levels double upon acute HFD and given the dramatic metabolomic rewiring induced by microglial palmitate exposure, we asked whether aMMR might also occur in other brain regions. We FACS-sorted cortical and hippocampal microglia and tested for mitochondrial activation (MMR) in 3d HFD exposed mice. Indeed, 3d HFD exposure triggered an increase in mitochondrial membrane potential in both cortical and hippocampal microglia (**Fig 5B-C**). These data were consistent with the CSF results and suggested therefore that acute high-fat feeding might alter higher cognitive function.

Given the hippocampal signature, we tested whether 3d HFD mice showed any deleterious memory phenotype compared to chow-fed controls. Surprisingly, HFD-treated animals outperformed the controls. Using a standard Barnes test, 3d HFD mice exhibited a faster reaction (**Fig 5D**), suggestive of improved learning and spatial memory. Similarly, when challenged with a T-Maze, 3d HFD exposed animals exhibited heightened spatial memory (**Fig 5E**). These phenotypes were reproducible at two different institutes (VAI, USA and MPI-IE, Germany) and in the hands of different experimentalists (**Fig 5D-E, Suppl Fig S5C-D**). Notably, the memory differences were observed in the absence of any detectable changes to motor coordination (ROTAROD; **Fig 5F-H**). Thus, acute high-fat feeding triggers improvements in learning and spatial memory.

To validate that these 3d HFD induced cognitive effects were microglial aMMR dependent, we once again repeated experiments in microglia-depleted (PLX-5622) and *Drp1^{MGKO}* mice. Importantly, PLX-5622-treated animals failed to show any detectable memory improvements upon a 3d HFD (**Fig 5I-J**) indicating indeed that an intact microglial compartment is necessary for acute HFD enhancement of memory function. Likewise, 3d HFD exposure failed to trigger memory improvements in *Drp1^{MGKO}* mice (**Fig 5K**) indicating that the memory enhancing response, like the glucose homeostatic effect, is microglial DRP1-dependent. Again, no mice in any treatment group showed altered motor effects by ROTAROD (**Suppl FigS5 E-J**). Therefore, 3d HFD-triggered aMMR appears to constitute a generalized physiological response that optimizes dietary coupling to diverse central functions.

DISCUSSION

Our data identify a new role for microglial cells as a rapid metabolic sensor of dietary macronutrient composition, and as a relay that triggers cognitive and peripheral metabolic responses. One of the most intriguing results was the directionality of the rapid metabolic responses. Whereas a bulk of literature demonstrates adverse outcomes upon chronic HFD, both in the brain (microgliosis, inflammatory cytokine release, myeloid cell infiltration) and periphery (hyperglycemia, insulin resistance)[8, 9], our findings indicate that acute HFD initiates a distinct homeostatic response that supports cognitive function. From an evolutionary perspective, there are obvious benefits to partitioning energy use towards cognition once energy demands are well met. We find that aMMR results from direct uptake, processing, and release of fatty acid derived carbons, and demonstrate that microglia are capable of metabolizing fatty acids towards diverse intracellular and extracellular pools. One immediate question raised by this work is the mechanistic nature of the flip from the seemingly beneficial acute MMR (aMMR) observed here, to the well-documented inflammatory MMR (iMMR) triggered after 1-2 weeks of chronic HFD. One possibility is that the response requires flexibility between lipid storage and processing, and that this becomes saturated with prolonged HFD.

Of equal interest are the PLX5622 experiments and data, which demonstrate for the first time that microglial ablation has no overt effect on baseline metabolism and memory. Importantly, however, the data show that microglia are critical for optimal response to dietary change. We are aware of the fact that CSFR1 inhibiting compounds such as PLX5622 deplete not only microglia but also long living CNS macrophages in the meninges and perivascular space [29] but they are by far less numerous and placed far from neurons in the parenchyma. We demonstrate a novel role for microglia in optimizing glycemia upon short- (2 hours) but not long- (24 hour) term fasting and therefore suggest that microglia mediate a glucose-sparing function in the transition from the post-prandial to fasted state. Future work mapping the downstream neuronal circuitry governing this response will be important. The overabundance of food in since industrialization has skewed a significant global population towards chronic prandial and post-prandial states and away from one of substantial intermittent fasting events. The finding that aMMR coordinates central metabolic balance with peripheral glucose homeostasis selectively during the prandial/post-prandial phase adds nuance to a significant literature distinguishing these physiological contexts [30], [31], [32]). From an evolutionary perspective it is easy to rationalize why initial periods of plenty would be mechanistically coupled to maximizing central functions.

One question raised by these findings is if there is a hierarchy for substrate sharing between glial cell (microglia, tanycytes, oligodendrocytes and astrocytes) and neurons. Our data indicate that microglia provide several TCA-associated substrates into the extracellular milieu, and, that palmitate/HFD increases this activity. Tanycytes and astrocytes have both been documented to release select metabolites into the extracellular environment [33, 34]. Given that CSF production is only loosely compartmentalized (e.g. relative to the highly physically structured control of blood), we suspect a cooperative model over hierarchical, serial or synergistic metabolic compartmentalization models. Other new questions relate to

the depth or breadth of other cognitive processes that might also be influenced by acute HFD. In this study, we demonstrate that aMMR involves release of at least 4 important anapleurotic substrates, and that aMMR is detectable from the hypothalamus to the hippocampus and cortex. Increased lactate has been shown to enhance fear memory in a glutamate-associated mechanism ([35]). Both lactate and glutamate are increased upon 3d HFD-induced aMMR.

In addition to identifying novel substrate routing patterns in microglia, our data demonstrate that mitochondrial fission is necessary for aMMR. Fatty acid triggered fission has been observed in several cell types [36] including neurons and glial cells [37],[38],[10]. Work by Kim et al. [10] suggests that the aMMR characterized here may require UCP2; those authors demonstrated UCP2-dependent mitochondrial changes in short- and long-term HFD exposed hypothalamic microglia. Collectively the two studies argue against the notion that astrocytes are unique amongst glial cells in their ability to use fatty acids, and importantly, to release fatty-acid derived substrates for use by neurons and other neighboring cells [39].

Finally, this study demonstrates previously unappreciated plasticity and complexity for microglial cellular metabolism. Rather than being largely glucose-constrained, our tracer studies reveal that primary microglia from across the brain readily take-up, metabolize and store fatty acids and that fatty acids are metabolized towards bioenergetic and acetylation reactions (acetyl-coA). They prove for the first time that substantial β-oxidation occurs in microglia cells even in the presence of high extracellular glucose [40]. The coordinate observations of intra- and extracellular succinate and itaconate accumulation and relative Complex II inhibition indicate that palmitate metabolism drives feed-forward inhibition of Complex II via itaconate production and shunting of TCA intermediates out of the cycle towards glutamate. Further examination of the role of glutamine as a fuel and anapleurotic regulator of cellular function is therefore warranted. At least under the standard conditions used here and, in the field, microglia appear to be metabolically wired release of carbon substrates to neighboring cells, through several intermediates including lactate, succinate, glutamate, citrate and itaconate. This idea is consistent with the lack of substantial induction of lipid droplet accumulation, respiration, or ROS buildup upon palmitate exposure.

In conclusion, we identify a rapid microglial mechanism that translates direct dietary fat sensation into a non-transcriptional, mitochondrial response that specifically alters extracellular regulatory substrates (lactate, glutamate, itaconate and succinate) and enhances memory function. The response is progressive over the first days of dietary intervention, an effect that appears dependent on feed forward inhibition of mitochondrial complex II by itaconate. The aMMR response is detectable across the entire brain, which carries important implications for understanding how our diet directly regulates diverse cognitive and homeostatic responses, and the development of pharmacological and lifestyle interventions to enhance them.

MATERIAL AND METHODS

Experimental Animals

All animal studies and experimental procedures were approved by the either the Max Planck Commities in Germany or by the Van Andel Institute Institutional Animal Care and Use Committee in US, before project initiation. All mice were housed in a temperature-controlled environment (23°C) with a 12-h light and 12-h dark (07.00–19.00) photoperiod. Animals were provided standard chow diet (Research Diets #5021; 23,6% calories from fat; Mouse Breeder Diet #6539) or HFD (60% fat; Research diet, Rodent Chow #D12492) and water ad libitum unless otherwise stated.

For the experiments performed on non-modified mice, C57BL/6J were purchased from Jackson Laboratory. $Drp1$ floxed mice $(Drp1^{fl/fl})$ and Cx3cr1^{CreER} mice (B6.129P2(C)-Cx3cr1$^{tm2.1(cre/ERT2)Jung}$/J) were purchased from Jackson Laboratory. Mice expressing tamoxifen-inducible Cre recombinase (CreERT2) in cells expressing CX3CR1 (Cx3cr1-cre:ERT2) were crossed with mice harboring conditional alleles Drp1 $(Drp1^{fl/fl})$. For induction of Cre recombinase, 5- to 6-week-old $Drp1^{MGKO}$ $(Drp1^{fl/fl}$-Cx3cr1-cre) mice and their littermate control, were treated with 4 mg tamoxifen (TAM, Sigma) solved in 200 µl corn oil (Sigma) injected subcutaneously at two time points 48 h apart. High fat diet (HFD) was started 4 weeks from the last injection to allow the replacement of peripheral monocytes [21]. Mice were sacrificed at different time points during the diet. Only males were used in this study.

Microglial Depletion

Microglia were depleted in all cases by feeding mice custom diet (Research Diets) containing the CSF1R inhibitor PLX5622 (Plexxikon) formulated in the exact diets indicated above. The compound-containing diets have the new order numbers (D12450: PLX5622-containing standard diet and D21021905: PLX5622-containing high-fat diet). PLX5622 was included to achieve a dose of 1.2 g/kg based on average adult C57BL/6J food intake. Animals were administered the diet for 7-9 days.

Microglia Cultures

Eight to ten mice (1–3 days old, mixed sex) from C57BL/6J mice were used for primary microglia culture. In brief, brains were dissected and placed in a small culture dish that contained a small volume of

Dulbecco's modified eagle medium (DMEM). The meningeal lining (dura and arachnoid layers) were then gently removed using two small straight forceps under a magnifying glass. The cleaned brain was then placed in a new culture dish minced into a fine slurry using a pair of corneal scissors. Suspended cells were filtered (70 μm) and centrifuged for 5 min at 1000 rpm and the pellet was re-suspended and plated on poly-D-lysine (Cat# P6407, Sigma)-coated 75cm^2 flasks with DMEM containing 1% penicillin-streptomycin, 10% fetal bovine serum. Seven to 10 days later, the flasks were stimulated for 3 days with 30ng/ml M-CSF (Cat# 315-02, Peprotech) and then, shaken (200 rpm) for 3 hours (37°C) to specifically release microglia.

Embryonic Cortical Neuron Culture Protocol
Primary neuron cultures were prepared from embryonic day 18 (E18) CD1 mice. Brains were gently removed from the embryos and placed into a petri dish filled with ice cold, sterile Hibernate Medium (Cat#. A1247601, Gibco). Hemispheres were gently separated, and the meninges, thalamus, striatum, brainstem, and hippocampus were removed. Cortical tissue was isolated and cut into 1 mm^3 segments. The cortical tissue from each brain was pooled and digested in papain solution (20 U/mL Cat# LS003126, Worthington) and then treated with DNase I (Cat# LS006563, Worthington) to remove residual DNA. The tissue was then washed with pre-warmed Neurobasal media (Cat# 21103049, Gibco), mechanically dissociated, and strained through a 40 μm cell strainer. The cell suspension was pelleted at 1000 rpm for 5 minutes, resuspended in 2 mL of neuron media (Neurobasal media containing 1% B27, 2mM GlutaMAX and penicillin-streptomycin) and gently mixed. The dissociated neurons were seeded on poly-D-lysine coated 6 well culture plates at 1 million cells/ well. On DIV3, cytosine arabinoside (1-β-D-arabinofuranosylcytosine) was added to a final concentration of 5 μM to curb glial proliferation. The neurons were maintained until DIV21 by replacing 1/3 volume of media with fresh neuron media every five days.

Microglia Isolation
Mice were anesthetized and blood was collected by ventricular puncture. Mice were then perfused with phosphate-buffered saline (PBS). For microglia isolation, the hypothalamus, cerebellum, hippocampus, and cortex were dissected from the brain and manually dissociated in HBSS buffer. A cell suspension was prepared with a continuous 37% Percoll gradient at 2300 rpm for 30 min without brake, then cells were washed with 1x PBS and resuspended in FACS buffer and non-specific binding to Fc receptors was blocked by incubation with anti-CD16/32 antibody (BD Pharmingen, Cat# 553141) and the FACS antibodies BV711 conjugated anti-CD11b and Pacific blue conjugated anti-CD45 antibodies (Cat# 101241, Cat# 103126, BioLegend).

Single-cell RNA-sequencing (ScRNA-seq)
For the single-cell RNAseq experiments, pure hypothalamic microglia cells were sorted and processed as previously described [41, 42].
Briefly, brains were isolated and gently homogenized and resuspended in 20 ml of ice-cold extraction buffer (1x HBSS, 1% fetal calf serum, 1 mM EDTA). Microglial cells were extracted in 5 ml of 37% isotonic Percoll. After staining, single CD45^{lo}, CD11b$^+$ microglial cells were FACS-sorted directly in 192-

well plates, containing 192 unique barcodes, for scRNA-seq. The CEL-Seq2 method was used for single cell sequencing [43, 44]. Thirteen libraries (2492 single cells) were sequenced on an Illumina HiSeq 2500 system, as pair-end multiplexing run, with 50-75 bp read length.

scRNA-seq analysis

The scRNA-seq libraries were analyzed using the 'scRNAseq' module from snakePipes v.1 [45]. Within the snakePipes pipeline, trimming of barcodes was achieved using Cutadapt v.1.9.1 [46]. Quality of the reads was evaluated with FastQC (https://www.bioinformatics.babraham.ac.uk/projects/fastqc/). Mapping to the GRCm38/mm10 mouse genome was performed using the STAR aligner v.2.5.3a [47], and read counts on features were quantified by featureCounts v.1.6.1 [48]. Mapped and counted read were next analyzed with RaceID3 v.0.2.6, with default parameters [44, 49]. Batch correction by plate, and preprocessing of data were completed within the RaceID3 pipeline. We included in our analysis, all microglia cells from control (CT) and 3-day high fat diet treated (3d_HFD) mice. We filtered out all the cells with a total transcript count per cell >1000. Dimensional reduction of transcriptomic profiles was then preformed with Uniform Manifold Approximation and Projection (UMAP). As a comparative analysis, we also added to our dataset, previously published single microglial cells from experimental autoimmune encephalomyelitis (EAE), and matched controls mice (CT_EAE) [42].

Data availability

The scRNA-seq raw data, processed count matrices and related metadata have been deposited to Gene Expression Omnibus (GEO) and are publicly available under the accession codes GSE217045.

qPCR

For the qPCR experiments, pure microglia cells were sorted, and the RNA was extracted with Trizol (ImGen protocol).

	Foward	Reverse
Tmem119	GTGTCTAACAGGCCCCAGAA	AGCCACGTGGTATCAAGGAG
P2ry12	CAAGGGGTGGCATCTACCTG	AGCCTTGAGTGTTTCTGTAGGG
Arg1	GGAAATCGTGGAAATGAG	CAGATATGCAGGGAGTCACC
S100B	AACAACGAGCTCTCTCACTTCC	CTCCATCACTTTGTCCACCA
RPL19	GAAGGTCAAAGGGAATGTGTTCA	CCTTGTCTGCCTTCAGCTTGT

Mitochondrial Function by Cytometry

For the mitochondrial activity experiments, the cell suspension was incubated with the mitochondrial probes MitoTracker Green FM (Invitrogen, Cat# M7514) and MitoTracker DeepRed FM (Invitrogen, Cat# 22426) for 30min at 37degrees before FACS acquisition. For the electron transport chain experiments (ETC), the cell suspension was incubated with the mitochondrial probe Tetramethylrhodamine TMRM (Abcam, Cat# ab228569) and fluorescent glucose analog 2-NBDG (Abcam, Cat# 235976) for 30min at 37degrees before FACS acquisition. For challenging the ETC, the cell suspension was incubated each 90 seconds by the following drugs: 0,5ul of 100uM Rotenone (Sigma),

2ul of 2.5M Succinate (Sigma) and 0.5ul of 1mM Antimycin (Sigma). Cytometry was performed on Fortessa (BD Bioscience) and analyzed with FlowJo v 10 (Treestar). Microglial cells were gated from CD45low-CD11b+ cells followed by singlet after forward and side scatter pattern.

Confocal Microscopy Analysis

Mice were anesthetized and transcardially perfused with 0.9% saline followed by fixative (4% paraformaldehyde). Brains were incubated 24hours with the fixative, then 48h with 20% sucrose and finally fixed with Polyfreeze (Sigma). Frozen brains were sliced into 7um and incubated in 0.1%PBST + 5%BSA with anti-Iba1 antibody (diluted 1:300, Abcam; Cat#ab178846) and/or anti-GFP antibody (diluted 1:200, Cell signaling; Cat#2255), or anti-DRP1 antibody (diluted 1:50 Cell signaling; Cat#8570). After several washes with PBS, sections were incubated in the appropriated secondary antibodies (thermofisher) for 1 hr at room temperature, then rinsed in PBS three times 10 min each time, and flat-embedded in mounting media with DAPI (Fluoroshield, Abcam; Cat#104139).
The Pictures acquisition were performed with the Confocal LSM780 (Zeiss).

Glucose and Insulin Tolerance

OGTTs were performed in 16 hours fasted animals. After determination of basal blood glucose levels, each animal received a gavage of 1g/kg glucose (Sigma) and blood glucose levels were measured at -30, 0, 15, 30, 45, 60, 90 and 120 min after glucose administration using a glucometer (Accu-Check, Roche). In the same cohort of mice, blood samples were also collected for determination of circulating insulin levels during the OGTT at -30, 15, 30 and 60 with the Elisa insulin assay kit (Mercodia).
ITTs were performed in 2 hours fasted animal. After determination of basal blood glucose levels, each animal received an i.p. injection of Insulin, 0.75 U/kg (Actrapid, Novo Nordisk). Blood glucose levels were measured at -30, 0, 15, 30, 45, 60, 90 and 120 min after insulin administration.

Body Composition

Body composition was measured in vivo by MRI (EchoMRI; Echo Medical Systems, Houston, TX).

Behavioral Tests

Mice were fasted at 7:00 AM and the behavioral tests were performed between 8:00 AM and 2:00 PM. ROTAROD, Barnes and T Maze behavioral tests were performed as previously described [50] [51].

Microglial Analysis

To analyze microglial number and size in the ARC, VMH and cortex, tdtomato positive cells were counted manually from 4 hypothalamic level-matched sections per animal using ImageJ software and microglia cell size was measured using a thresholding parameter on ImageJ software. A total of 40 cells per section were used to determine the size in all regions.

Measures of Mitochondrial length

Primary microglial cells were seeded overnight in Poly-D-lysine-coated cell culture chambered coverslips (Lab-Tek Cat#155411, Thermo scientific) at $1x10^4$ cells/well density in 100 µl microglial growth media. Then, they were incubated at 37 for 2, 6 or 24 hrs in microglial growth media completed with 100uM BSA or 100uM Palmitate complexed with BSA [52] or 100uM Oleate complexed with BSA or 1ug/ml LPS [53]. Half hour before the end of the incubation, 200nM MitoTrakerGreen (Invitrogen, Cat# M7514) was added in the media. The cells were washed 3 times with their own incubation media and the mitochondrial network was observed in vivo cells with Confocal LSM 780 (Zeiss).

After pictures acquisition, 5uM MitoSox (Invitrogen, Cat# M36008) were added in the incubated media for 10min. Cells were washed 3 times with media and fixed with 4%PFA at 37 for 15min. The ROS staining was observed with Confocal LSM 780 (Zeiss).

After pictures acquisition, cells were permeabilized with 0.2%Triton in PBS, incubated with blocking buffer (PBS + 5%FCS +0,1%Tween) for 1 hour and stained with anti-Iba1 antibody (diluted 1:300, Abcam; Cat#ab178846) and /or anti-TOM20 antibody (diluted 1:1000, SantaCruz; Cat#sc177615) or/and anti-DRP1 antibody (diluted 1:50 Cell signaling; Cat#8570). After several washes with PBS, sections were incubated in the appropriated secondary antibodies (thermofisher) for 1 hour at room temperature, then rinsed in PBS three times 10 min each time, the pictures acquisition were performed with the Confocal LSM780 (Zeiss).

Cytokine measurement

Media from primary Microglia incubated with BSA or Palmitate was collected and processed using the mouse Custom Panel Standard kit (#93976 LegendPlex)

Stable isotope labeling and metabolomics

Metabolomics was performed on microglia by first washing microglia primary cell cultures with PBS and re-cultured in DMEM (lacking glucose) containing 10% dialyzed FBS and uniformly labeled [^{13}C]-Glucose (Cambridge Isotope Laboratories). Microglia (2×10^6 per well in 6 well plates) were cultured in ^{13}C-containing medium for up to 6 hours. For cellular media samples, 10 µL of media were taken at indicated time points and centrifuged to remove cells, with 10 µL of media used for metabolite analysis. For uniformly labeled [^{13}C]-Palmitate tracing analysis, sodium [^{13}C]-Palmitate was conjugated to BSA following Agilent Seahorse Palmitate-BSA conjugation protocol. For [^{13}C]-Palmitate tracing, microglia primary cell cultures were first cultured for 24hr with BSA control or ^{12}C-Palmitate (200uM) in DMEM containing 10% dialyzed FBS. Following 24hr incubation, the media was removed, and microglia cells washed with PBS followed by culture in DMEM with 10% dialyzed FBS and blank mM [^{13}C]-Palmitate for 4 hours and cell and media samples collected as before.

For Gas chromatography coupled to mass spectrometry (GC-MS) metabolites were extracted using ice cold 80% methanol, sonicated, and then D-myristic acid was added (750ng/sample) as an internal standard. Dried samples were dissolved in 30 µL methozyamine hydrochloride (10mg/ml) in pyridine and derivatized as tert-butyldimethylsily (TBDMS) esters using 70 µL N-(*tert*-butyldimethylsilyl)-N-

methyltrifluoroacetamide (MTBSTFA) [54]. For metabolite analysis, an Agilent 5975C GC/MS equipped with a DB-5MS+DG (30 m x 250 μm x 0.25 μm) capillary column (Agilent J&W, Santa Clara, CA, USA) was used. All data were collected by electron impact set at 70 eV. A total of 1 μL of the derivatized sample was injected in the GC in splitless mode with inlet temperature set to 280˚C, using helium as a carrier gas with a flow rate of 1.5512 mL/min (rate at which myristic acid elutes at 17.94 min). The quadrupole was set at 150˚C and the GC/MS interface at 285˚C. The oven program for all metabolite analyses started at 60˚C held for 1 min, then increased at a rate of 10˚C/min until 320˚C. Bake-out was at 320˚C for 10 min. Sample data were acquired both in scan (1-600 m/z) modes. MassHunter software (v10, Agilent Technologies) was used for peak picking and integration of GCMS data. Peak areas of all isotoplogues for a molecular ion of each metabolite were used for mass isotopomer distribution anaylsis using a custom algorithm developed at VAI. Briefly, the atomic composition of the TBDMS-derivatized metabolite fragments (M-57) was determined, and matrices correcting for natural contribution of isotopomer enrichment were generated for each metabolite. After correction for natural abundance, a comparison was made between non-labeled metabolite abundances (^{12}C) and metabolite abundances which were synthesized from the ^{13}C tracer. Metabolite abundance was expressed relative to the internal standard (D-myristic acid) and normalized to cell number.

For liquid chromatography coupled to mass spectrometry (LC-MS) metabolites Metabolites were analyzed for relative abundance by high resolution accurate mass detection (HRAM) on two QExactive™ Orbitrap mass spectrometers (Thermo Fisher Scientific) coupled to Thermo Vanquish liquid chromatography systems. Separate instruments were used for negative and positive mode analysis. For negative mode analysis, an Acquity T3 HSS (1.8 μm, 2.1 mm x 150 mm) column (Waters, Eschborn, Germany) was used for chromatographic separation and the elution gradient was carried out with a binary solvent system. Solvent A consisted of 3% methanol, 10 mM tributylamine, and 15mM acetic acid in water (pH 5.0 +/- 0.05) and solvent B was 100% methanol. A constant flow rate of 200 μL min^{-1} was maintained and the linear gradient employed was as follows: 0–2.5 min 100% A, 2.5–5 min increase from 0 to 20% B, 5–7.5 min maintain 80% A and 20% B, 7.5–13 min increase from 20 to 55% B, 13–15.5 min increase from 55 to 95% B, 15.5–18.5 min maintain 5% A and 95% B, 18.5–19 min decrease from 95 – 0% B, followed by 6 min of re-equilibration at 100% A. The heater temperature was set to 400° C and ion spray voltage was set to 2.75 kV. The column temperature was maintained at 25 °C and sample volumes of 10 μL were injected. A 22-minute full-scan method was used to acquire data with *m/z* scan range from 80 to 1200 and resolution of 70,000. The automatic gain control (AGC) target was set at 1e6 and the maximum injection time was 500 ms. For positive mode analysis, an Atlantis T3 (3 μm, 2.1mm ID × 150mm) column (Waters) was used and the he elution gradient was carried out with a binary solvent system Solvent A consisted of 0.1% acetic acid and 0.025% heptafluorobutyric acid in water and solvent B was 100% acetonitrile. A constant flow rate of 400 μL min−1 was maintained and the linear gradient employed was as follows: 0–4 min increase from 0 to 30% B, 4–6 min from 30 to 35% B, 6–6.1 min from 35 to 100% B and hold at 100% B for 5min, followed by 5 min of re-equilibration. The heater temperature was set to 300° C and the ion spray voltage was set to 3.5 kV. The column temperature was maintained at 25 °C and sample volumes of 10 μL were injected. An 11-minute full-scan method was used to acquire data with *m/z* scan range from 70 to 700 and resolution of 70,000. The automatic gain control (AGC)

target was set at 1e6 and the maximum injection time was 250 ms. Instrument control and acquisition was carried out by Xcalibur 2.2 software (Thermo Fisher Scientific). Full scan LC-MS data were analyzed in Compound Discoverer (v 3.2, Thermo Scientific). Compounds were identified by chromatography specific retention time of external standards and MS^2 spectral matching using the mzCloud database (Thermo Scientific).

Quantification and Statistical Analysis

Two-way ANOVA was used to determine the effect of the genotype and treatment with the Prism 7.01 software (GraphPad Software). For repeated measures analysis, ANOVA was used when values over different times were analyzed. When only two groups were analyzed, statistical significance was determined by an unpaired Student's t-test. A value of $p < 0.05$ was considered statistically significant. All data are shown as mean ± SEM unless stated otherwise. We did not include additional statistical tests for data distributions.

1.   Kleinridders, A., A.C. Konner, and J.C. Bruning, *CNS-targets in control of energy and glucose homeostasis.* Curr Opin Pharmacol, 2009. **9**(6): p. 794-804.
2.   Grayson, B.E., R.J. Seeley, and D.A. Sandoval, *Wired on sugar: the role of the CNS in the regulation of glucose homeostasis.* Nat Rev Neurosci, 2013. **14**(1): p. 24-37.
3.   Argente-Arizon, P., et al., *Glial cells and energy balance.* J Mol Endocrinol, 2017. **58**(1): p. R59-R71.
4.   Pellerin, L., et al., *Evidence supporting the existence of an activity-dependent astrocyte-neuron lactate shuttle.* Dev Neurosci, 1998. **20**(4-5): p. 291-9.
5.   Magistretti, P.J. and I. Allaman, *Lactate in the brain: from metabolic end-product to signalling molecule.* Nat Rev Neurosci, 2018. **19**(4): p. 235-249.
6.   Belanger, M., I. Allaman, and P.J. Magistretti, *Brain energy metabolism: focus on astrocyte-neuron metabolic cooperation.* Cell Metab, 2011. **14**(6): p. 724-38.
7.   Suzuki, A., et al., *Astrocyte-neuron lactate transport is required for long-term memory formation.* Cell, 2011. **144**(5): p. 810-23.
8.   Thaler, J.P., et al., *Obesity is associated with hypothalamic injury in rodents and humans.* J Clin Invest, 2012. **122**(1): p. 153-62.
9.   Valdearcos, M., et al., *Microglial Inflammatory Signaling Orchestrates the Hypothalamic Immune Response to Dietary Excess and Mediates Obesity Susceptibility.* Cell Metab, 2017. **26**(1): p. 185-197 e3.
10.   Kim, J.D., et al., *Microglial UCP2 Mediates Inflammation and Obesity Induced by High-Fat Feeding.* Cell Metab, 2019. **30**(5): p. 952-962 e5.
11.   Yi, C.X., et al., *TNFalpha drives mitochondrial stress in POMC neurons in obesity.* Nat Commun, 2017. **8**: p. 15143.
12.   Vinuesa, A., et al., *Early Exposure to a High-Fat Diet Impacts on Hippocampal Plasticity: Implication of Microglia-Derived Exosome-like Extracellular Vesicles.* Mol Neurobiol, 2019. **56**(7): p. 5075-5094.
13.   Hao, S., et al., *Dietary obesity reversibly induces synaptic stripping by microglia and impairs hippocampal plasticity.* Brain Behav Immun, 2016. **51**: p. 230-239.
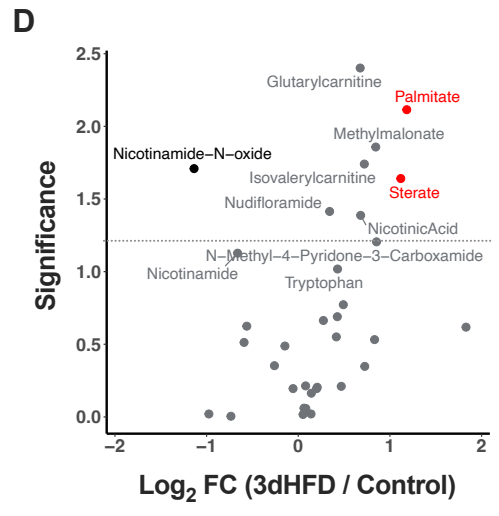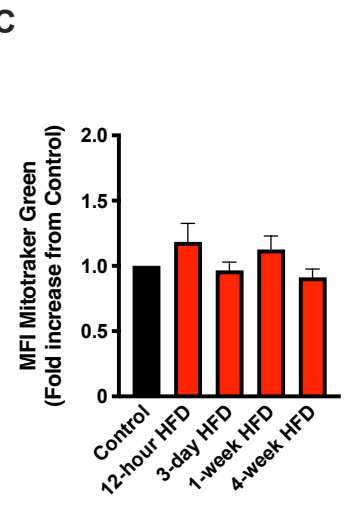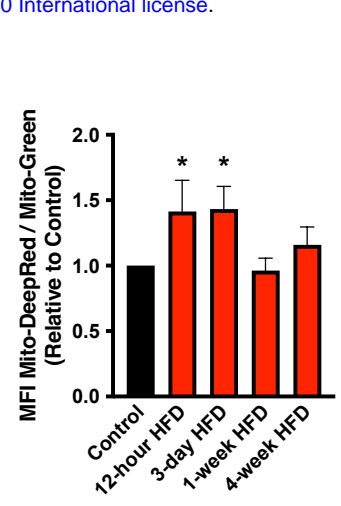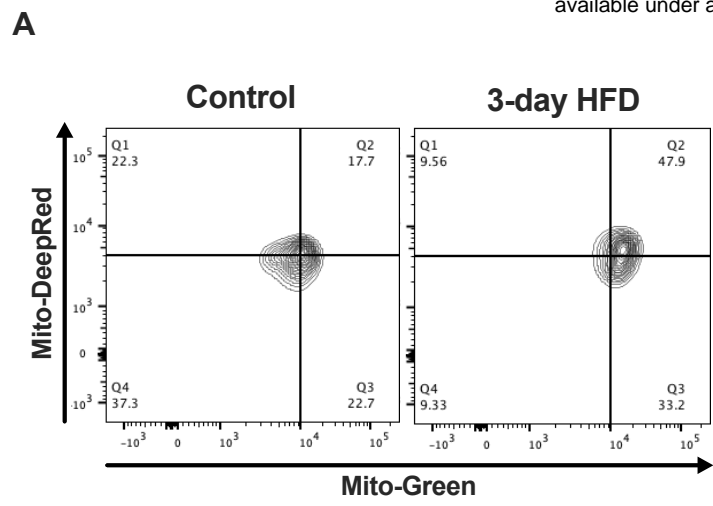
14. Spencer, S.J., et al., *High-fat diet and aging interact to produce neuroinflammation and impair hippocampal- and amygdalar-dependent memory.* Neurobiol Aging, 2017. **58**: p. 88-101.

15. Duffy, C.M., et al., *High fat diet increases cognitive decline and neuroinflammation in a model of orexin loss.* Neurobiol Learn Mem, 2019. **157**: p. 41-47.

16. Benani, A., et al., *Food intake adaptation to dietary fat involves PSA-dependent rewiring of the arcuate melanocortin system in mice.* J Neurosci, 2012. **32**(35): p. 11970-9.

17. Wang, J., et al., *Overfeeding rapidly induces leptin and insulin resistance.* Diabetes, 2001. **50**(12): p. 2786-91.

18. Gregor, M.F. and G.S. Hotamisligil, *Inflammatory mechanisms in obesity.* Annu Rev Immunol, 2011. **29**: p. 415-45.

19. Feng, X., et al., *Microglia mediate postoperative hippocampal inflammation and cognitive decline in mice.* JCI Insight, 2017. **2**(7): p. e91229.

20. Pearce, E.L., et al., *Fueling immunity: insights into metabolism and lymphocyte function.* Science, 2013. **342**(6155): p. 1242454.

21. Goldmann, T., et al., *A new type of microglia gene targeting shows TAK1 to be pivotal in CNS autoimmune inflammation.* Nat Neurosci, 2013. **16**(11): p. 1618-26.

22. Wakabayashi, J., et al., *The dynamin-related GTPase Drp1 is required for embryonic and brain development in mice.* J Cell Biol, 2009. **186**(6): p. 805-16.

23. Gao, Y., et al., *Hormones and diet, but not body weight, control hypothalamic microglial activity.* Glia, 2014. **62**(1): p. 17-25.

24. Ackermann, W.W. and V.R. Potter, *Enzyme inhibition in relation to chemotherapy.* Proc Soc Exp Biol Med, 1949. **72**(1): p. 1-9.

25. Hooftman, A. and L.A.J. O'Neill, *The Immunomodulatory Potential of the Metabolite Itaconate.* Trends Immunol, 2019. **40**(8): p. 687-698.

26. Pellerin, L., *How astrocytes feed hungry neurons.* Mol Neurobiol, 2005. **32**(1): p. 59-72.

27. Bouzier-Sore, A.K., et al., *Competition between glucose and lactate as oxidative energy substrates in both neurons and astrocytes: a comparative NMR study.* Eur J Neurosci, 2006. **24**(6): p. 1687-94.

28. Waterson, M.J. and T.L. Horvath, *Neuronal Regulation of Energy Homeostasis: Beyond the Hypothalamus and Feeding.* Cell Metab, 2015. **22**(6): p. 962-70.

29. Goldmann, T., et al., *Origin, fate and dynamics of macrophages at central nervous system interfaces.* Nat Immunol, 2016. **17**(7): p. 797-805.

30. Dakic, T.B., et al., *Short-term fasting promotes insulin expression in rat hypothalamus.* Eur J Neurosci, 2017. **46**(1): p. 1730-1737.

31. Havel, P.J., *Peripheral signals conveying metabolic information to the brain: short-term and long-term regulation of food intake and energy homeostasis.* Exp Biol Med (Maywood), 2001. **226**(11): p. 963-77.

32. Zeltser, L.M., R.J. Seeley, and M.H. Tschop, *Synaptic plasticity in neuronal circuits regulating energy balance.* Nat Neurosci, 2012. **15**(10): p. 1336-42.

33. Garcia-Caceres, C., et al., *Role of astrocytes, microglia, and tanycytes in brain control of systemic metabolism.* Nat Neurosci, 2019. **22**(1): p. 7-14.

34. Barca-Mayo, O. and M. Lopez, *Astrocyte Clocks and Glucose Homeostasis.* Front Endocrinol (Lausanne), 2021. **12**: p. 662017.

35. Ikeda, H., S. Yamamoto, and J. Kamei, *Increase in brain l-lactate enhances fear memory in diabetic mice: Involvement of glutamate neurons.* Brain Res, 2021. **1767**: p. 147560.

36.   Buck, M.D., et al., *Mitochondrial Dynamics Controls T Cell Fate through Metabolic Programming.* Cell, 2016. **166**(1): p. 63-76.

37.   Schneeberger, M., et al., *Mitofusin 2 in POMC neurons connects ER stress with leptin resistance and energy imbalance.* Cell, 2013. **155**(1): p. 172-87.

38.   Ramirez, S., et al., *Mitochondrial Dynamics Mediated by Mitofusin 1 Is Required for POMC Neuron Glucose-Sensing and Insulin Release Control.* Cell Metab, 2017. **25**(6): p. 1390-1399 e6.

39.   Westergaard, N., U. Sonnewald, and A. Schousboe, *Metabolic trafficking between neurons and astrocytes: the glutamate/glutamine cycle revisited.* Dev Neurosci, 1995. **17**(4): p. 203-11.

40.   Kalsbeek, M.J., L. Mulder, and C.X. Yi, *Microglia energy metabolism in metabolic disorder.* Mol Cell Endocrinol, 2016. **438**: p. 27-35.

41.   Tay, T.L., et al., *A new fate mapping system reveals context-dependent random or clonal expansion of microglia.* Nat Neurosci, 2017. **20**(6): p. 793-803.

42.   Tay, T.L., et al., *Unique microglia recovery population revealed by single-cell RNAseq following neurodegeneration.* Acta Neuropathol Commun, 2018. **6**(1): p. 87.

43.   Hashimshony, T., et al., *CEL-Seq2: sensitive highly-multiplexed single-cell RNA-Seq.* Genome Biol, 2016. **17**: p. 77.

44.   Herman, J.S., Sagar, and D. Grun, *FateID infers cell fate bias in multipotent progenitors from single-cell RNA-seq data.* Nat Methods, 2018. **15**(5): p. 379-386.

45.   Bhardwaj, V., et al., *snakePipes: facilitating flexible, scalable and integrative epigenomic analysis.* Bioinformatics, 2019. **35**(22): p. 4757-4759.

46.   Martin, M., *Cutadapt removes adapter sequences from high-throughput sequencing reads.* 2011, 2011. **17**(1): p. 3.

47.   Dobin, A., et al., *STAR: ultrafast universal RNA-seq aligner.* Bioinformatics, 2013. **29**(1): p. 15-21.

48.   Liao, Y., G.K. Smyth, and W. Shi, *featureCounts: an efficient general purpose program for assigning sequence reads to genomic features.* Bioinformatics, 2014. **30**(7): p. 923-30.

49.   Grun, D., *Revealing dynamics of gene expression variability in cell state space.* Nat Methods, 2020. **17**(1): p. 45-49.

50.   Shiotsuki, H., et al., *A rotarod test for evaluation of motor skill learning.* J Neurosci Methods, 2010. **189**(2): p. 180-5.

51.   Illouz, T., R. Madar, and E. Okun, *A modified Barnes maze for an accurate assessment of spatial learning in mice.* J Neurosci Methods, 2020. **334**: p. 108579.

52.   Valdearcos, M., et al., *Microglia dictate the impact of saturated fat consumption on hypothalamic inflammation and neuronal function.* Cell Rep, 2014. **9**(6): p. 2124-38.

53.   Katoh, M., et al., *Polymorphic regulation of mitochondrial fission and fusion modifies phenotypes of microglia in neuroinflammation.* Sci Rep, 2017. **7**(1): p. 4942.

54.   Faubert, B., et al., *Loss of the tumor suppressor LKB1 promotes metabolic reprogramming of cancer cells via HIF-1alpha.* Proc Natl Acad Sci U S A, 2014. **111**(7): p. 2554-9.
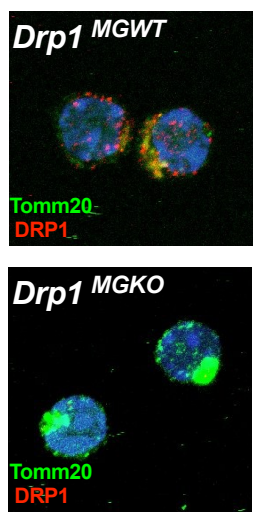
Figure_1
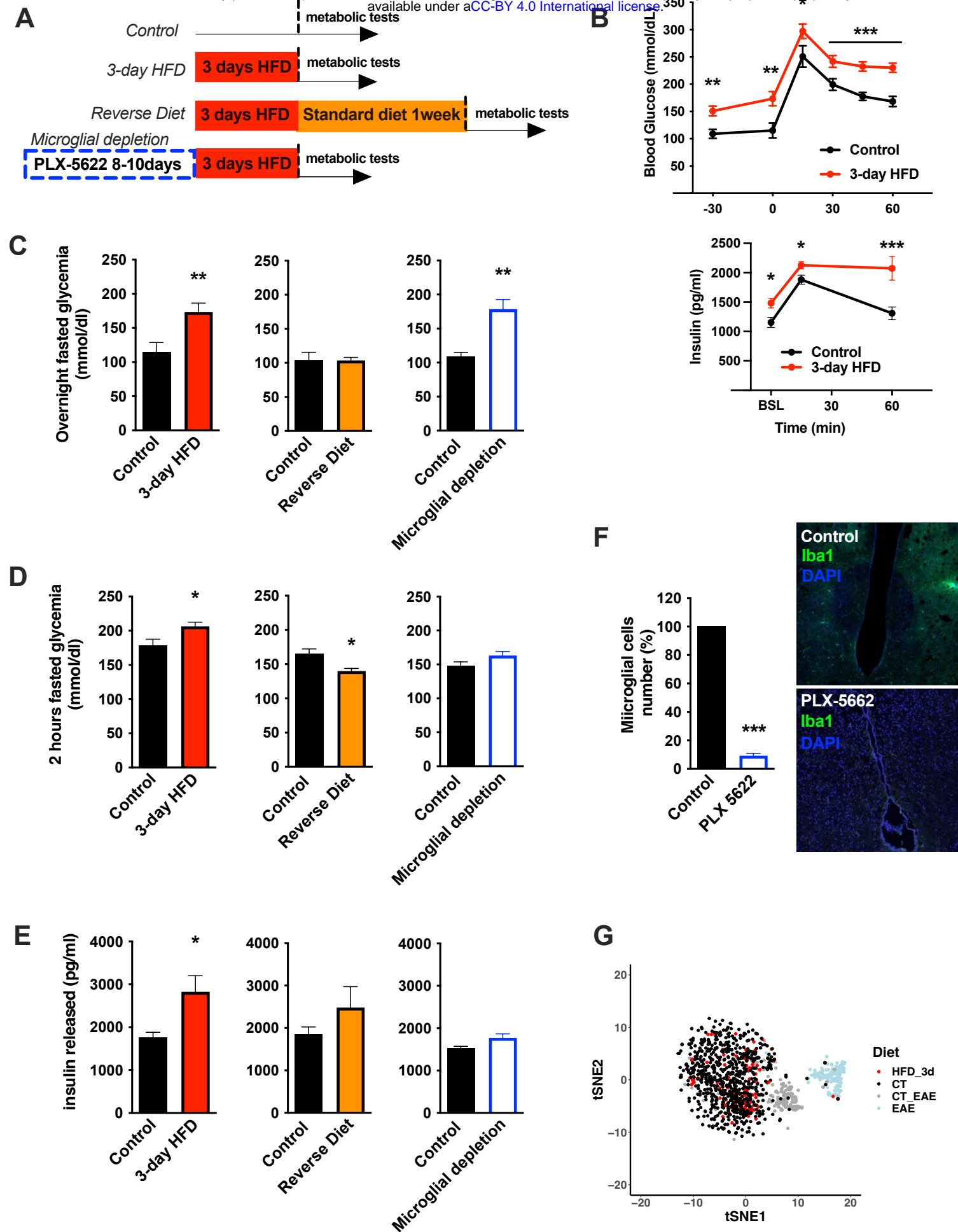
Metabolite	FC	log2FC	P.value	log10.P.Value	Enrichment
KynurenicAcid	3.56	1.83	0.24	0.62	Not Sig
HexadecanoicAcid	2.27	1.18	0.01	2.11	HFD 3d
Nicotinamide-N-oxide	0.45	-1.14	0.02	1.71	CT
OctadecanoicAcid	2.17	1.12	0.02	1.64	HFD 3d
Serotonin	0.51	-0.98	0.95	0.02	Not Sig
N-Methyl-4-Pyridone-3-Carboxamide	1.81	0.85	0.06	1.21	Not Sig
Methylmalonate	1.80	0.85	0.01	1.86	Not Sig
TetradecanoicAcid	1.78	0.83	0.29	0.53	Not Sig
Octanoylcarnitine	0.60	-0.73	0.99	0.00	Not Sig
Propionylcarnitine	1.65	0.73	0.45	0.35	Not Sig
Isovalerylcarnitine	1.65	0.72	0.02	1.74	Not Sig
NicotinicAcid	1.60	0.68	0.04	1.39	Not Sig
Glutarylcarnitine	1.60	0.68	0.00	2.40	Not Sig
Nicotinamide	0.63	-0.66	0.07	1.13	Not Sig
1-methylnicotinamide	0.66	-0.59	0.31	0.51	Not Sig
OphthalmicAcid	0.68	-0.56	0.24	0.62	Not Sig
N-methylserotonin	1.41	0.49	0.17	0.77	Not Sig
O-Acetylcarnitine	1.38	0.47	0.62	0.21	Not Sig
Tryptophan	1.35	0.43	0.10	1.02	Not Sig
3-hydroxyanthranillicAcid	1.34	0.43	0.20	0.69	Not Sig
Butyrylcarnitine	1.33	0.42	0.28	0.55	Not Sig
Nudifloramide	1.27	0.34	0.04	1.41	Not Sig
QuinolinicAcid	1.21	0.27	0.22	0.66	Not Sig
S-Adenosyl-L-Homocysteine	0.84	-0.26	0.44	0.35	Not Sig
Isobutyrylcarnitine	1.15	0.21	0.62	0.20	Not Sig
2-MethylbutyrylCarnitine	1.15	0.20	0.64	0.19	Not Sig
NicotinicAcidMononucleotide	0.90	-0.15	0.33	0.49	Not Sig
Hexanoylcarnitine	1.10	0.14	0.69	0.16	Not Sig
NicotinamideMononucleotide	1.10	0.14	0.95	0.02	Not Sig
Carnitine	1.06	0.08	0.88	0.06	Not Sig
S-Adenosyl-L-Methionine	1.06	0.08	0.61	0.21	Not Sig
3-Hyroxykynurenine	1.04	0.06	0.87	0.06	Not Sig
NicotinuricAcid	0.96	-0.06	0.64	0.19	Not Sig
AnthranillicAcid	1.04	0.05	0.96	0.02	Not Sig

TABLE_1

A

B

C

D

E

F

G

H

Figure_2

0 KB

Drp1^{MGWT} *Drp1^{MGKO}*

Tomm20
DRP1

Drp1^{MGKO}

D

Overnight fasted glycemia (mmol/dl)

Overnight fasted glycemia (mmol/dl)
250 / 200 / 150 / 100 / 50 / 0
Drp1^{MGWT} *Drp1^{MGKO}*

2 hours fasted glycemia (mmol/dl)
250 / 200 / 150 / 100 / 50 / 0
DRP1 WT DRP1 KO

2 hours fasted glycemia (mmol/dl)
250 / 200 / 150 / 100 / 50 / 0
Drp1^{MGWT} *Drp1^{MGKO}*

insulin released (pg/ml)
4000 / 3000 / 2000 / 1000 / 0
DRP1 WT DRP1 KO

insulin released (pg/ml)
4000 / 3000 / 2000 / 1000 / 0
Drp1^{MGWT} *Drp1^{MGKO}*

E

Overnight fasted glycemia (mmol/dl)
250 / 200 / 150 / 100 / 50 / 0
DRP1 WT DRP1 KO

Overnight fasted glycemia (mmol/dl)
250 / 200 / 150 / 100 / 50 / 0
Drp1^{MGWT} *Drp1^{MGKO}*

2 hours fasted glycemia (mmol/dl)
300 / 200 / 100 / 0
DRP1 WT DRP1 KO
**

2 hours fasted glycemia (mmol/dl)
Drp1^{MGWT} *Drp1^{MGKO}*
**

insulin released (pg/ml)
4000 / 3000 / 2000 / 1000 / 0
Drp1^{MGWT} *Drp1^{MGKO}*

insulin released (pg/ml)
4000 / 3000 / 2000 / 1000 / 0
DRP1 WT DRP1 KO
*

Figure_3

Figure_4

A

Neuronal tracer uptake

B

Cortex

C

Hippocampus

D **E** **F** **G** **H**

I **J** **K**

Figure_5

FIGURE 1: Acute HFD-induced metabolic changes are microglia dependent

A. Schematic depicting the different treatments and diets followed by the different mice groups.

B. Graphs showing the Glucose Tolerance Test (OGTT) and the associated-insulin kinetic of C57Bl6/J male fed with control diet (Control) or fed with high fat diet for 3 days (3-day HFD) (n=8).

C. Graph showing the overnight fasted glycemia from the mice groups depicting in the **A.** Schematic (n=5 to 11).

D. Graph showing the 2hours-fasted glycemia from the mice groups depicting in the **A.** schematic (n=5 to 11).

E. Graph showing the insulin released after a glucose gavage from the mice groups depicting in the **A.** schematic (n=5 to 11).

F. Microglial cells staining with Iba1 (green) in the brain slices from mice fed with 3 days HFD or mice depleted from their microglial cells with 1 week control diet complexed with PLX-5662 prior the 3 days HFD (PLX-5662) (n=5).

G. sgRNAseq dataset from hypothalamic microglia cells harvested from C57bl6/J male mice fed with control diet (CT) and High Fat Diet for 3 days (HFD_3d) (n=5) merged with sgRNAseq microglia dataset from mice presenting an Experimental Autoimmune Encephalomyelitis (EAE).

Data are presented as mean ±SEM. *p<0.05, **p<0.01, ***p<0.001 as determined by two-tailed Student's test and two-way ANOVA followed by Bonferroni post hoc test.

FIGURE 2: A rapid Microglial Mitochondria Response to high fat diet

A. Facs plots depicting the ratio Mitotraker Deep Red/ Mitotraker Green from sorted microglial cells of C57Bl6/J male fed with a control diet (Control) or fed with high fat diet for 3 days (3-day HFD).

B. Graph showing the ratio Mitotraker Deep Red/ Mitotraker Green from sorted hypothalamic microglial cells of C57Bl6/J male fed with a control diet (Control) or fed with high fat diet for 12 hours,3 days or 1-4 weeks (n=5 to 12).

C. Graph showing the Mitotraker Green fluorescence from sorted hypothalamic microglial cells of C57Bl6/J male fed with a control diet (Control) or fed with high fat diet for for 12 hours,3 days or 1-4 weeks (n=5 to 12).

D. Volcano plot showing the metabolites content of cerebrospinal fluid from of C57Bl6/J male fed with a control diet (Control) or fed with high fat diet for 3 days (n=10).

E. Seahorse (+/- succinate added in the media during the experiment) on primary microglia challenged for 24hours with BSA (control) or Palmitate (experiment replicated 3times).

F. Mitochondrial Electron transport chain activity recorded with FACS after TMRM staining from sorted microglial cells of C57Bl6/J male fed with a control diet (Control) or fed with high fat diet for 3 days (n=5).

G. Mitochondrial networks from primary microglia stained with Mitotraker green after being challenged for 24hours with BSA (control), Palmitate, Oleate or LPS (n=40) and the mitochondrial length quantification graphs.

H. DRP1 colocalization with the mitochondrial network stained with TOMM20 on primary microglial cell after being challenged for 24hours with BSA (control) and Palmitate(n=40) and the colocalization quantification graphs.

Data are presented as mean ±SEM. *p<0.05, **p<0.01, ***p<0.001 as determined by two-tailed Student's test and two-way ANOVA followed by Bonferroni post hoc test.

FIGURE 3: aMMR is required for diet induced homeostatic rewiring *in vivo*
A. Immunostaining of TOMM20 and DRP1 on sorted microglia from mice $Drp1^{MGWT}$ or $Drp1^{MGKO}$
B. Western Blot against DRP1 on sorted microglia from mice $Drp1^{MGWT}$ or $Drp1^{MGKO}$
C. Graphs showing the overnight fasted glycemia, the 2hours fasted glycemia and the insulin released from $Drp1^{MGWT}$ or $Drp1^{MGKO}$ fed with control diet (n=5 to 11).
D. Graphs showing the overnight fasted glycemia, the 2hours fasted glycemia and the insulin released from $Drp1^{MGWT}$ or $Drp1^{MGKO}$ fed with 3 day high fat diet (n=5 to 11).
Data are presented as mean ±SEM. *p<0.05, **p<0.01, ***p<0.001 as determined by two-tailed Student's test and two-way ANOVA followed by Bonferroni post hoc test.

FIGURE 4: Palmitate induces a novel microglial lactate/succinate/itaconate release pathway.
A. BODIPY staining on primary microglia challenged for 24hours with BSA or palmitate and the lipid droplets quantification graph. (n=20)
B. Schematic depicting the timeline for the tracing experiments (^{13}C-palmitate or ^{13}C-glucose) on primary microglial challenged for 24hours with BSA or palmitate.
C. ^{13}C-palmitate incorporation into palmytoilcarnitine (m+16) and acetylcarnitine (m+2) after 4 hours tracing experiment on primary microglia pretreated for 24hours with BSA or palmitate (n=3).
D. ^{13}C-palmitate incorporation into acetyl serine (m+2) after 4 hours tracing experiment on primary microglia pretreated for 24hours with BSA or palmitate (n=3).
E. ^{13}C-palmitate incorporation into aconitate, alpha-ketoglutarate, fumarate, malate (m+2) after 4 hours tracing experiment on primary microglia pretreated for 24hours with BSA or palmitate (n=3).
F. ^{13}C-palmitate incorporation into glutamate (m+2) after 4 hours tracing experiment on primary microglia pretreated for 24hours with BSA or palmitate (n=3).
G. ^{13}C-palmitate incorporation into glutamate (m+2) released during the 4 hours tracing experiment by primary microglia pretreated for 24hours with BSA or palmitate (n=3). The results are graphed in relative abundance.
H. ^{13}C-palmitate incorporation into itaconate (m+1) released during the 4 hours tracing experiment by primary microglia pretreated for 24hours with BSA or palmitate (n=3).
I. ^{13}C-palmitate incorporation into succinate (m+2) released during the 4 hours tracing experiment by primary microglia pretreated for 24hours with BSA or palmitate (n=3).
J. ^{13}C-glucose incorporation into the intracellular glucose pool (m+6) after 6 hours tracing experiment on primary microglia pretreated for 24hours with BSA or palmitate (n=3).
K. ^{13}C-glucose incorporation into glutamate (m+2) released during the 6 hours tracing experiment by primary microglia pretreated for 24hours with BSA or palmitate (n=3).
L. ^{13}C-glucose incorporation into itaconate (m+1) released during the 6 hours tracing experiment by primary microglia pretreated for 24hours with BSA or palmitate (n=3).

M. ^{13}C-glucose incorporation into succinate (m+2) released during the 6 hours tracing experiment by primary microglia pretreated for 24hours with BSA or palmitate (n=3).

N. ^{13}C-glucose incorporation into lactate (m+3) released during the 6 hours tracing experiment by primary microglia pretreated for 24hours with BSA or palmitate (n=3).

O. Schematic depicting the metabolic pathways used by the primary microglial challenged for 24hours with BSA (black arrow) or palmitate (red arrow) during the different tracing (^{13}C-palmitate or ^{13}C-glucose).

Data are presented as mean ±SEM. *p<0.05, **p<0.01, ***p<0.001 as determined by two-tailed Student's test and two-way ANOVA followed by Bonferroni post hoc test.

FIGURE 5: Acute HFD induces widespread MMR and rapid modulation of spatial and learning memory

A. Primary microglial cell media was collected after the ^{13}C-glucose tracing (containing ^{13}C-lactate released by microglia challenged with BSA or Palmitate) and incubated for 4 hours with primary neurons, the graph shows the ^{13}C-lactate incorporation in the neurons in relative abondance, as control, primary neurons were incubated directly with ^{13}C-glucose (n=6).

B. Graph showing the ratio Mitotraker Deep Red/ Mitotraker Green from sorted cortical microglial cells of C57Bl6/J male fed with a control diet (Control) or fed with high fat diet for 3 days (3-day HFD) (n=5 to 12).

C. Graph showing the ratio Mitotraker Deep Red/ Mitotraker Green from sorted hippocampic microglial cells of C57Bl6/J male fed with a control diet (Control) or fed with high fat diet for 3 days (3-day HFD) (n=5 to 12).

D. Graph showing the latency during the Barnes Test from mice fed with normal diet (Control) or 3 days HFD (3-day HFD) (n=11). The test was performed in the VAI animals facility (USA).

E. Graph showing the alternation during the T Maze Test from mice fed with normal diet (Control) or 3 days HFD (3-day HFD) (n=11). The test was performed in the VAI animals facility (USA).

F. Graph showing the distance walked during the ROTAROD test from mice fed with normal diet (Control or 3 days HFD (3-day HFD) (n=11).

G. Graph showing the number of turn before the mice fall during the ROTAROD test from mice fed with normal diet (Control) or 3 days HFD (3-day HFD) (n=11).

H. Graph showing the latency during the ROTAROD test from mice fed with normal diet (Control) or 3 days HFD (3-day HFD) (n=11).

I. Microglial staining with Iba1 (green) in the Hippocampus slices from mice fed with 3 days HFD or mice depleted from their microglial cells with 1 week control diet complexed with PLX-5662 prior the 3 days HFD (PLX-5662) (n=5).
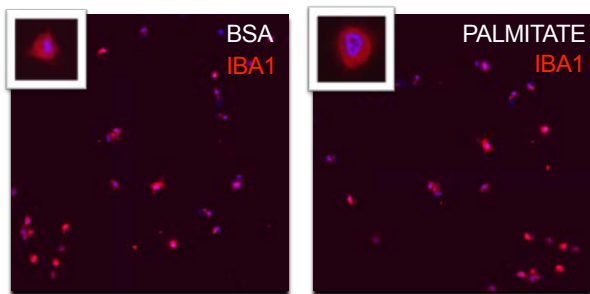
J. Graph showing the latency during the Barnes Test from mice fed with normal diet (Control) or with depleted microglia (n=8).

K. Graph showing the latency during the Barnes Test from *Drp1^{MGWT}* or *Drp1^{MGKO}* mice fed with normal diet (Control diet) or with 3 days HFD (3-day HFD) (n=11).
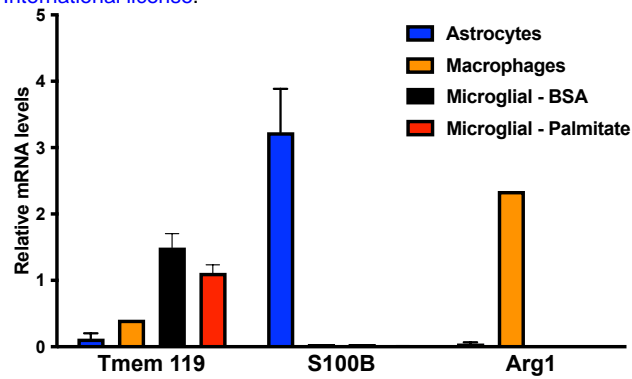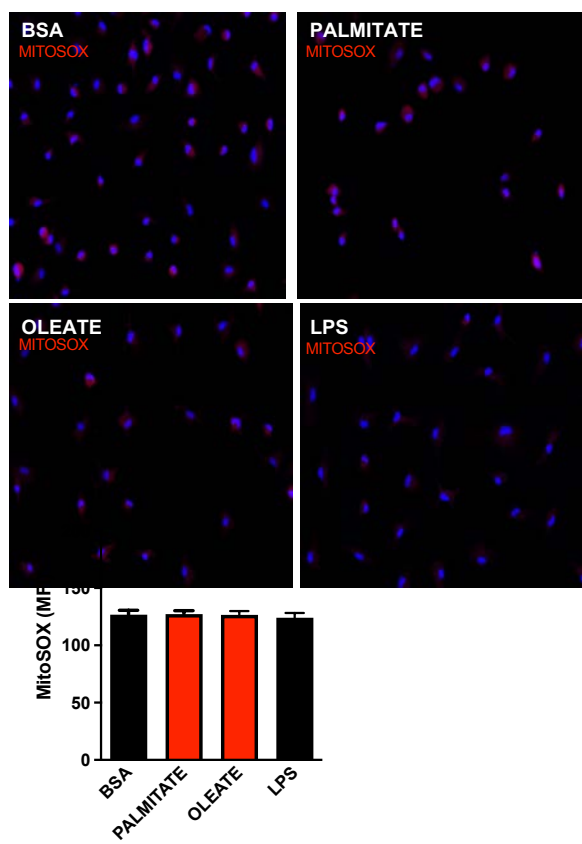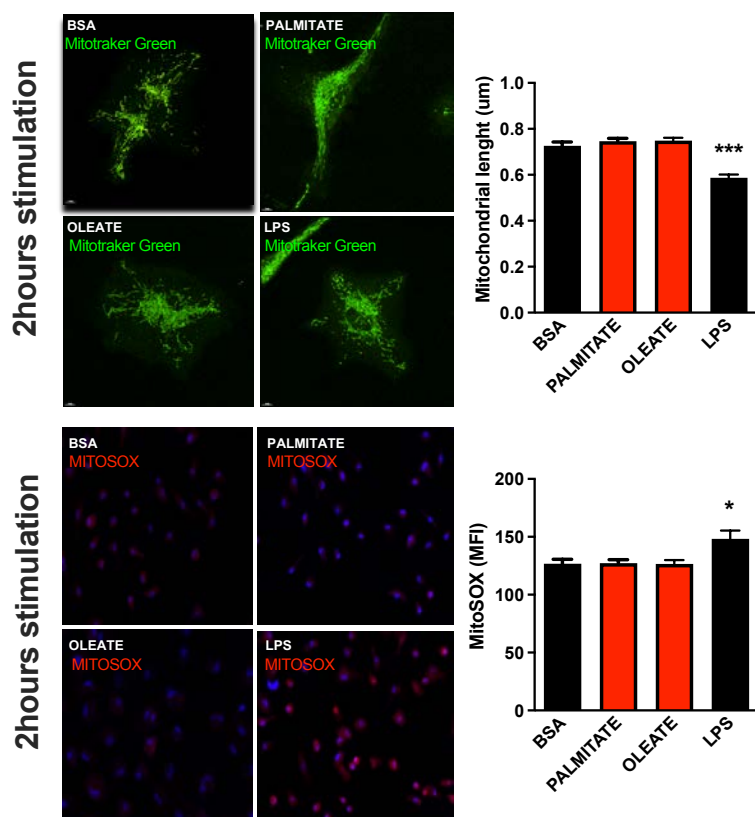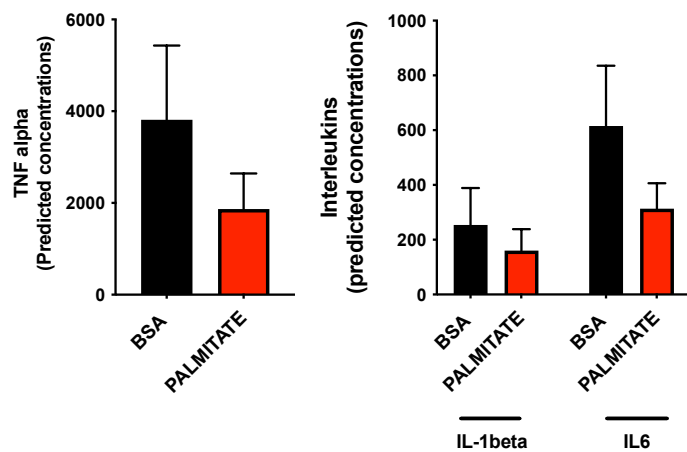
Data are presented as mean ±SEM. *p<0.05, **p<0.01, ***p<0.001 as determined by two-tailed Student's test and two-way ANOVA followed by Bonferroni post hoc test.

Supp_Figure_1

Supp_Figure_2

A

B

C

D

PRE - DIETS   3 DAYS HIGH FAT DIET

Supp_Figure_3

Supp_Figure_4

A

Primary neurons
Map2
NeuN
Iba1

Primary neurons
Map2
NeuN
GFAP

B

(Microglial media)   (Neuronal pellet)
U-[^{13}C]-Substrates → Citrate

(Microglial media)   (Neuronal pellet)
U-[^{13}C]-Substrates → Itaconate

(Microglial media)   (Neuronal pellet)
U-[^{13}C]-Substrates → Succinate

***

M+0
M+1
M+2
M+3
M+4
M+5

Rel. Abundance

U-[^{13}C]-GLUCOSE   BSA   PALMITATE

Conditionned medias
from U-[^{13}C]-labelled microglia

C Latency to hole (sec) — Control, 3-day HFD *

D Alternation rate (AU) — Control, 3-day HFD *

E Distance (cm) — Control, Microglial depletion

F Fall (rpm) — Control, Microglial depletion

G Latency (sec) — Control, Microglial depletion

H Distance (cm) — Drp1^{MGWT}, Drp1^{MGKO} (Control Diet); Drp1^{MGWT}, Drp1^{MGKO} (3-day HFD)

I Fall (rpm) — Drp1^{MGWT}, Drp1^{MGKO} (Control Diet); Drp1^{MGWT}, Drp1^{MGKO} (3-day HFD)

J Latency (sec) — Drp1^{MGWT}, Drp1^{MGKO} (Control Diet); Drp1^{MGWT}, Drp1^{MGKO} (3-day HFD)

Supp_Figure_5
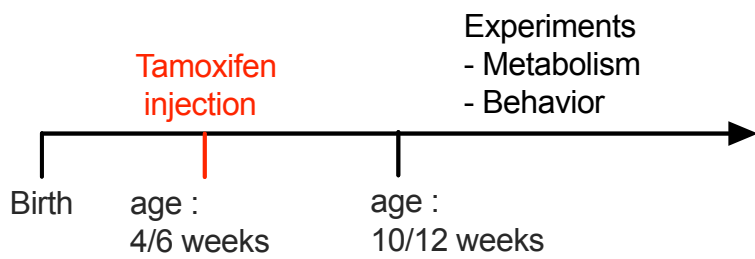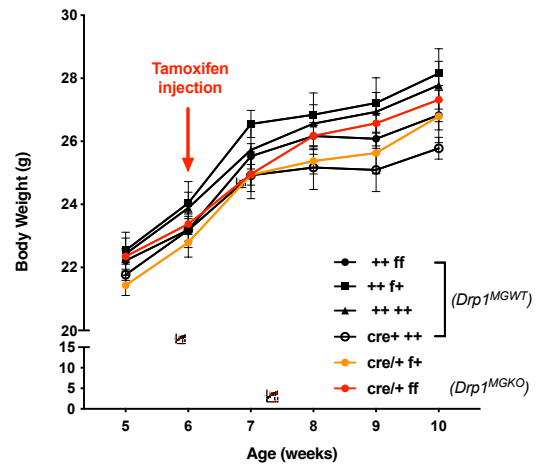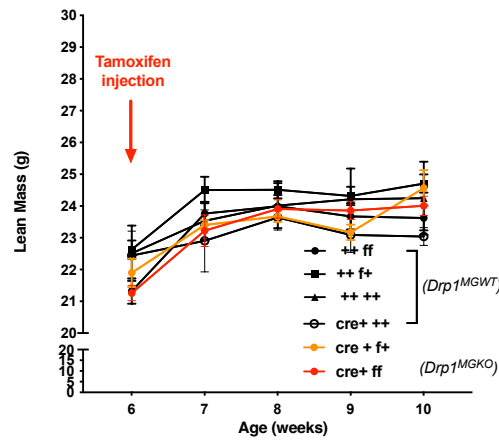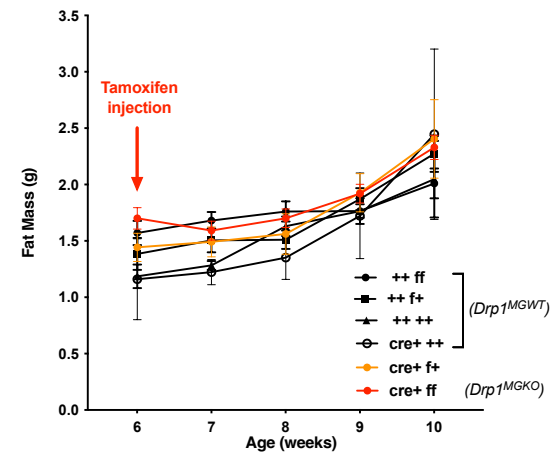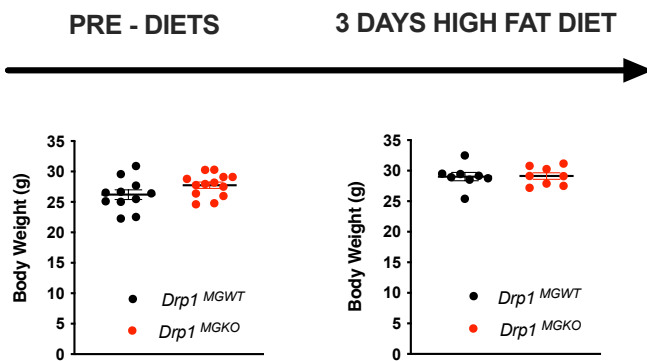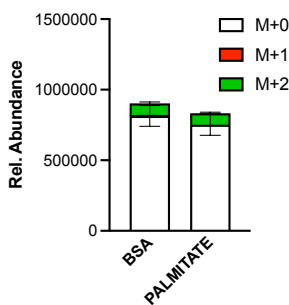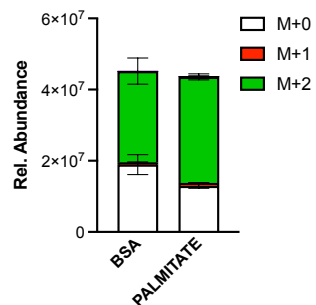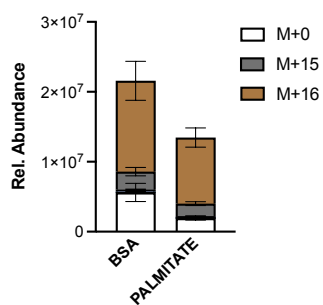
SUPPL FIGURE 1: Acute HFD-induced metabolic changes are microglia dependent

A. Graphs showing the Glucose Tolerance Test (OGTT) and the associated-insulin kinetic of C57Bl6/J male before keeping them with a control diet (Control) or before feeding them with high fat diet for 3 days (3-day HFD) (n=8).

B. Graph showing the Insulin Tolerance Test (ITT) of C57Bl6/J male before keeping them with a control diet (Control) or before feeding them with high fat diet for 3 days (3-day HFD) (n=5).

C. Graphs showing the Glucose Tolerance Test (OGTT) expressed in percentage from the basal glycemia of C57Bl6/J male fed with a control diet (Control) or fed with high fat diet for 3 days (3-day HFD) (n=8).

D. Graph showing the body weight evolution between C57Bl6/J male fed with control diet (Control) or fed with high fat diet for 3 days (3-day HFD), before and after the diet change. (n=7).

E. IBA1 immunostaining on hypothalamic slices from C57Bl6/J male fed with control diet (Control) or fed with high fat diet for 3 days (3-day HFD) and its quantification (n=10).

F. IBA1 and YFP immunostaining on hypothalamic slices from Cx3cr1creERT2-Rosa26YFP mice fed with control diet or 3 days high fat diet for 3 days (n=5).

G. sgRNAseq dataset from hypothalamic microglia cells harvested from C57bl6/J male mice fed with control diet (Control) and High Fat Diet for 3 days (HFD_3d) (n=5)

Data are presented as mean ±SEM. *$p<0.05$, **$p<0.01$, ***$p<0.001$ as determined by two-tailed Student's test and two-way ANOVA followed by Bonferroni post hoc.

SUPPL FIGURE 2: A rapid Microglial Mitochondria Response to high fat diet

A. IBA1 immunostaining of primary microglia cells treated with BSA (control) or Palmitate for 24hours.

B. Graph showing mRNA expression of microglial marker (TMEM119) or astrocytes marker (S100B) or macrophages marker (Arg1) in primary microglial culture challenged for 24hours with BSA or palmitate. Primary culture of astrocytes and macrophages were used as positive controls.

C. MitoSOX staining of primary microglial cells after being challenged for 24hours with BSA (control), Palmitate, Oleate or LPS (n=10) and the MitoSOX quantification graph.

D. Mitochondrial networks from primary microglia stained with Mitotraker green and stained with MitoSOX after being challenged for 2hours with BSA (control), Palmitate, Oleate or LPS (n=40) and the mitochondrial length as well as the MitoSOX quantification graphs

F. Interleukins concentrations (TNFalpha, IL-1beta, IL6) in the primary microglia cells media after being challenged for 24hours with BSA or palmitate (n=7)

Data are presented as mean ±SEM. *$p<0.05$, **$p<0.01$, ***$p<0.001$ as determined by two-tailed Student's test and two-way ANOVA followed by Bonferroni post hoc.

SUPPL FIGURE 3: aMMR is required for diet induced homeostatic rewiring *in vivo*

A Schematic depicting the timeline for the tamoxifen injection and the experiments performed on *Drp1^{MGWT}* or *Drp1^{MGKO}*

B. Graph showing the body weight evolution among all the *Drp1^{MGKO}* genotypes after the tamoxifen injection (n=6 to 11)

C. Graphs showing the fat mass and lean mass evolution among all the *Drp1^MGKO^* genotypes after the tamoxifen injection (n=6 to 11)

D. Graphs showing the body weight before and after the 3 day HFD for the mice *Drp1^MGWT^* and *Drp1^MGKO^* (n=11 to 13)

Data are presented as mean ±SEM. *p<0.05, **p<0.01, ***p<0.001 as determined by two-tailed Student's test and two-way ANOVA followed by Bonferroni post hoc.

SUPPL FIGURE 4: Palmitate induces a novel microglial lactate/succinate/itaconate release pathway.

A ^{13}C-palmitate incorporation into palmytoilcarnitine and acetylcarnitine after 4 hours tracing experiment on primary microglia pretreated for 24hours with BSA or palmitate (n=3). The results are graphed in relative abundance.

B. ^{13}C-palmitate incorporation into acetyl-serine after 4 hours tracing experiment on primary microglia pretreated for 24hours with BSA or palmitate (n=3). The results are graphed in relative abundance.

C. ^{13}C-palmitate incorporation into aconitate, alpha-ketoglutarate, fumarate, malate after 4 hours tracing experiment on primary microglia pretreated for 24hours with BSA or palmitate (n=3). The results are graphed in relative abundance.

D. ^{13}C-palmitate incorporation into glutamate after 4 hours tracing experiment on primary microglia pretreated for 24hours with BSA or palmitate (n=3). The results are graphed in relative abundance.

E. ^{13}C-glucose incorporation into pyruvate, citrate, alpha-ketoglutarate, succinate, and malate after 6 hours tracing experiment on primary microglia pretreated for 24hours with BSA or palmitate (n=3). The results are graphed in pool size.

Data are presented as mean ±SEM. *p<0.05, **p<0.01, ***p<0.001 as determined by two-tailed Student's test and two-way ANOVA followed by Bonferroni post hoc.

SUPPL FIGURE 5: Acute HFD induces widespread MMR and rapid modulation of spatial and learning memory

A. Map2, NeuN, Iba1 and Map2, NeuN, GFAP immunostainings on primary neurons.

B. Primary microglial cell media was collected after the ^{13}C-glucose tracing (containing ^{13}C-metabolites released by microglia challenged with BSA or Palmitate) and incubated for 4 hours with primary neurons, the graph shows the ^{13}C-citrate, ^{13}C-itaconate and ^{13}C-succinate incorporation in the neurons in relative abondance (n=6).

C. Graph showing the latency during the Barnes Test from mice fed with normal diet (Control), or 3 days HFD (3-day HFD) (n=11). The test was performed in the MPI animals facility (Germany).

D. Graph showing the alternation during the T Maze Test from mice fed with normal diet (Control), or 3 days HFD (3-day HFD) (n=11). The test was performed in the MPI animals facility (Germany).

E. Graph showing the distance walked during the ROTAROD test from mice fed with normal diet (Control) or depleted from their microglia (n=8).

F. Graph showing the number of turns before the mice fall during the ROTAROD test from mice fed with normal diet (Control), (Control) or depleted from their microglia (n=8).

G. Graph showing the latency during the ROTAROD test from mice fed with normal diet (Control) or depleted from their microglia (n=8).

H. Graph showing the distance walked during the ROTAROD test from $Drp1^{MGWT}$ or $Drp1^{MGKO}$ mice fed with normal diet (Control diet), or 3 days HFD (3-day HFD) (n=11).

I. Graph showing the number of turns before the mice fall during the ROTAROD test from $Drp1^{MGWT}$ or $Drp1^{MGKO}$ mice fed with normal diet (Control diet), or 3 days HFD (3-day HFD) (n=11).

I. Graph showing the latency during the ROTAROD test from $Drp1^{MGWT}$ or $Drp1^{MGKO}$ mice fed with normal diet (Control diet), or 3 days HFD (3-day HFD) (n=11).

Data are presented as mean ±SEM. *p<0.05, **p<0.01, ***p<0.001 as determined by two-tailed Student's test and two-way ANOVA followed by Bonferroni post hoc.